ELIGULUM-A Regulates Lateral Branch and Leaf Development in Barley[1][OPEN]

Ron J. Okagaki,[a] Allison Haaning,[a] Hatice Bilgic,[a] Shane Heinen,[a] Arnis Druka,[b] Micha Bayer,[b] Robbie Waugh,[b] and Gary J. Muehlbauer[a,c,2]

[a]Department of Agronomy and Plant Genetics, University of Minnesota, St. Paul, Minnesota 55108
[b]James Hutton Institute, Dundee, United Kingdom
[c]Department of Plant and Microbial Biology, University of Minnesota, St. Paul, Minnesota 55108

ORCID IDs: 0000-0002-2065-3135 (R.J.O.); 0000-0002-3697-7177 (S.H.); 0000-0003-3663-2694 (A.D.); 0000-0003-0041-3115 (M.B.); 0000-0003-1045-3065 (R.W.); 0000-0001-9320-2629 (G.J.M.).

The shoot apical and axillary meristems control shoot development, effectively influencing lateral branch and leaf formation. The barley (*Hordeum vulgare*) *uniculm2* (*cul2*) mutation blocks axillary meristem development, and mutant plants lack lateral branches (tillers) that normally develop from the crown. A genetic screen for *cul2* suppressors recovered two recessive alleles of *ELIGULUM-A* (*ELI-A*) that partially rescued the *cul2* tillering phenotype. Mutations in *ELI-A* produce shorter plants with fewer tillers and disrupt the leaf blade-sheath boundary, producing liguleless leaves and reduced secondary cell wall development in stems and leaves. *ELI-A* is predicted to encode an unannotated protein containing an RNaseH-like domain that is conserved in land plants. *ELI-A* transcripts accumulate at the preligule boundary, the developing ligule, leaf margins, cells destined to develop secondary cell walls, and cells surrounding leaf vascular bundles. Recent studies have identified regulatory similarities between boundary development in leaves and lateral organs. Interestingly, we observed *ELI-A* transcripts at the preligule boundary, suggesting that *ELI-A* contributes to boundary formation between the blade and sheath. However, we did not observe *ELI-A* transcripts at the axillary meristem boundary in leaf axils, suggesting that *ELI-A* is not involved in boundary development for axillary meristem development. Our results show that *ELI-A* contributes to leaf and lateral branch development by acting as a boundary gene during ligule development but not during lateral branch development.

Leaves and tillers, the vegetative branches that form at the base of grass plants, are key determinants of grass shoot architecture. Tillers develop from axillary meristems and undergo three distinct morphological stages: (1) initiation of an axillary meristem in the leaf axil; (2) development of leaf primordia on the axillary meristem to form an axillary bud; and (3) elongation of internodes into a tiller with the potential to form a grain-bearing spike (Schmitz and Theres, 2005). Primary tillers form in leaf axils on the main stem, and secondary and higher order tillers form in axils of leaves on primary tillers and subsequent tillers, respectively. Grass leaves develop from the flanks of the shoot apical meristem and axillary meristems and are composed of a proximal sheath and distal blade divided by the ligular boundary. The ligular region is composed of the ligule, an outgrowth of an epidermal tissue flap, and the auricle. Auricles have two parts, a band of small cells separating the sheath from the blade and a flap of tissue growing out from the leaf margin that wraps around the stem in some species (Becraft et al., 1990; Sylvester et al., 1990). Both tillers and leaves are important agricultural traits for cereal crops and have been studied extensively (for review, see Wang and Li, 2008; Lewis and Hake, 2016; Mathan et al., 2016). However, our understanding of the interrelatedness of their genetic control is early in its fruition.

Positional information is important for morphogenesis, and boundaries between cell types often are the location of new tissue development. Thus, the role of boundary formation in axillary meristem development is an intense area of study (for review, see Žádníková and Simon, 2014; Hepworth and Pautot, 2015; Wang et al., 2016). The Arabidopsis (*Arabidopsis thaliana*) *REGULATORS OF AXILLARY MERISTEMS1* (*RAX1*) and *CUP-SHAPED COTYLEDON2* (*CUC2*) genes were identified by their expression pattern and reduced-branching

[1] This research was supported by a grant from the United States Department of Agriculture-CSREES-NRI Plant Growth and Development program grant # 2004-03440 and funds received from the Triticeae Coordinated Agricultural Project, U.S. Department of Agriculture/National Institute for Food and Agriculture grant number 2011-68002-30029 to G.J.M.

[2] Address correspondence to muehl003@umn.edu.

The author responsible for distribution of materials integral to the findings presented in this article in accordance with the policy described in the Instructions for Authors (www.plantphysiol.org) is: Gary J. Muehlbauer (muehl003@umn.edu).

R.J.O. performed most of the experiments and wrote the article; A.H. performed the RNA in situ hybridizations and edited the article; H.B. developed genetic materials; S.H. conducted the suppressor screen; A.D. and M.B. performed the bioinformatics analysis; R.W. oversaw the bioinformatics analysis and edited the article; G.J.M. conceived the original research plan and edited the article.

[OPEN] Articles can be viewed without a subscription.

www.plantphysiol.org/cgi/doi/10.1104/pp.17.01459

mutant phenotypes and were found to establish the boundary for axillary meristem development (Keller et al., 2006; Müller et al., 2006). Other boundary genes show the expected expression pattern but lack a clear axillary meristem phenotype in mutant plants. Plants overexpressing Arabidopsis *BLADE-ON-PETIOLE* (*BOP*) show a branching phenotype, producing extra paraclades in leaf nodes (Ha et al., 2007). The role of Arabidopsis *LATERAL ORGAN FUSION* (*LOF1*) in axillary meristem development was revealed by double mutants with its homolog, *LOF2* (Lee et al., 2009). The Arabidopsis *REGULATOR OF AXILLARY MERISTEM FORMATION1* (*ROX1*) has a subtle phenotype but is involved in axillary meristem development (Yang et al., 2012). However, the role of *ROX1* in axillary meristem development is more obvious in other species such as rice (*Oryza sativa*) and maize (*Zea mays*), highlighting the importance of comparative work to fully delineate developmental pathways (Komatsu et al., 2003; Gallavotti et al., 2004). These studies, and others, have identified genes acting in axillary meristem boundary formation, and it appears that a number of these genes help establish other developmental boundaries.

Boundary formation also is critical for leaf patterning (for review, see Bar and Ori, 2014; Lewis and Hake, 2016). Tomato (*Solanum lycopersicum*) plants produce compound leaves with several pairs of lateral leaflets and a terminal leaflet, with each leaflet having multiple lobes. *Goblet* (*Gob*) is one gene controlling this process, and *Gob* encodes a homolog of *CUC1/2* (Berger et al., 2009). *Gob* mutations also repress axillary meristem development (Busch et al., 2011). *Potato leaf* (*C*) and *blind* are recent duplications of the tomato *RAX1* homolog, and subfunctionalization of these duplicated genes gave *blind* a role in axillary meristem development and *C* a role in leaf development (Busch et al., 2011). In Arabidopsis, *CUC2* functions similarly to produce serrated leaves (Nikovics et al., 2006; Bilsborough et al., 2011). It is now evident that many of the same genes act to establish boundaries for meristem and leaf development (Hepworth and Pautot, 2015; Wang et al., 2016)

The identification of genes with dual roles in boundary demarcation and leaf and axillary meristem development prompted Busch and colleagues (2011) to propose a conserved genetic system that establishes axillary meristems and determines leaf shape. A related genetic system for maize leaf and lateral organ initiation was recently proposed as well (Johnston et al., 2014). Transcriptome analysis of laser-dissected tissues from the maize preligule region identified genes expressed at the blade-sheath boundary that are homologs of previously identified genes involved in lateral organ initiation (Johnston et al., 2014). Among the differentially expressed genes were the maize *CUC2* and *BOP* homologs. RNA in situ hybridization experiments showed maize *CUC2-like* transcripts accumulating in the preligule band, the cleft of developing ligules, and at the location of lateral branch initiation. The maize *BOP-like* transcripts accumulated in developing ligules, leaf axils, and axillary meristems (Johnston et al., 2014). The barley (*Hordeum vulgare*) *UNICULME4* (*CUL4*) gene is the barley *BOP* homolog (Tavakol et al., 2015), and plants carrying mutations in *CUL4* are defective in both axillary meristem and ligule development. In addition, *CUL4* is expressed in developing ligules, leaf axils, and axillary meristems and defines the boundaries of ligule and axillary bud development like the maize *BOP* homolog (Tavakol et al., 2015).

In this study, we conducted a genetic suppressor screen using a mutant that does not make tillers, *cul2* (Babb and Muehlbauer, 2003), and identified two mutations in the *ELIGULUM-A* (*ELI-A*) gene that promoted axillary meristem development and tillering in the *cul2* mutant background. Mutations in *ELI-A* have been described previously as pleiotropic, with altered ligule development, reduced plant height, weak culms, and compact spikes (Lundqvist and Franckowiak, 2002). Additional characterization showed that *eli-a* mutant plants exhibited reduced tillering and secondary cell wall formation compared with the nonmutant backcross parent line. We isolated the *ELI-A* gene and determined that it encodes a previously unannotated protein. RNA in situ hybridizations showed that *ELI-A* transcripts are found in the preligular region, the developing ligule, leaf margins, cells destined to develop secondary cell walls, and cells surrounding leaf vascular bundles. Taken together, these observations show that *ELI-A* plays a role in ligule and axillary meristem development. We propose that *ELI-A* functions in establishing a boundary during ligule development but not for axillary meristem development.

RESULTS AND DISCUSSION

Isolation and Genetic Characterization of *cul2* Suppressor Mutants

The barley *cul2* mutant rarely makes tillers due to its inability to produce axillary buds (Fig. 1; Babb and Muehlbauer, 2003). To identify suppressors of the *cul2* mutant phenotype, we mutagenized the Bowman-*cul2.b-rob1* stock. *Rob1* (orange lemma) is a phenotypic marker tightly linked to *cul2* (Franckowiak et al., 1997). Over 15,000 sodium azide-mutagenized, M3 Bowman-*cul2.b-rob1* families were screened for plants that produced tillers, and two recessive suppressor mutants were recovered. The two suppressors proved to be alleles of the previously described *ELI-A* gene (see below) and were named *eli-a.17* and *eli-a.18*. In Bowman-*eli-a.17; cul2.b-rob1* and Bowman-*eli-a.18; cul2.b-rob1* mutant plants, the uniculm phenotype of *cul2* was partially suppressed (Fig. 1). For example, in a greenhouse trial, 28 of 41 Bowman-*eli-a.17; cul2.b-rob1* plants produced one or two tillers with the remaining plants having no tillers, and all 21 Bowman-*eli-a.18; cul2.b-rob1* plants had one or more tillers (Supplemental Fig. S1). Unexpectedly, homozygous mutant *eli-a.18* plants were short with leaves that drooped and lacked ligules (Figs. 1 and 2), whereas these traits were not seen in *eli-a.17* plants (Figs. 1 and 2).

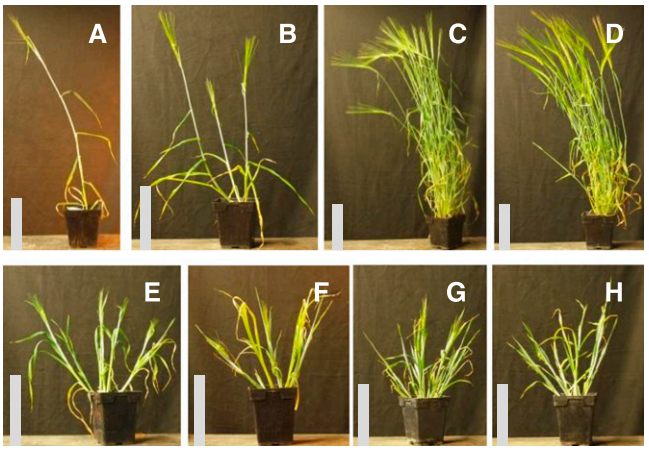

Figure 1. Mutant and nonmutant adult plant characteristics. A, Bowman-*cul2.b-rob1*. B, Bowman-*cul2.b-rob1; eli-a.17*. C, Nonmutant cv Bowman. D, Bowman-*eli-a.17*. E, Bowman-*eli-a.18*. F, *Bowman-cul2.b-rob1; eli-a.18*. G, *eli-a.14*. H, *cul2.b-rob1; eli-a.14*. The nonmutant cv Bowman and Bowman-*eli-a.17* plants in C and D were grown in the field and transferred to pots for photographs. Other plants were grown in a growth chamber. Bars = 20 cm.

To determine if *eli-a.17* and *eli-a.18* were allelic, seven crosses between Bowman-*cul2.b-rob1/cul2.b-rob1; eli-a.17/eli-a.17* and Bowman-*cul2.b-rob1/cul2.b-rob1; eli-a.18/eli-a.18* were made. Tillers were observed on 18 out of 19 F1 plants, demonstrating that the two suppressors were allelic (Supplemental Fig. S2). In the F2 plants, *eli-a.18* mutants exhibited stronger suppression of *cul2.b* than *eli-a.17*. Bowman-*eli-a.18; cul2.b-rob1* mutant plants were liguleless and developed an average of 2.9 tillers per plant compared with Bowman-*eli-a.17; cul2.b-rob1* plants, which developed ligules and had 0.8 tillers per plant (Supplemental Fig. S1). Finally, the heteroallelic combination of *eli-a.17/eli.a-18* exhibited an intermediate number of tillers in the *cul2.b* mutant background, 1.59 tillers per plant, and an intermediate liguleless phenotype (Fig. 2; Supplemental Figs. S1 and S3).

The *eli-a.17* and *eli-a.18* alleles also mapped to the same region on chromosome 2HS. We mapped *eli-a.17* using the *cul2* suppressor phenotype. The *eli-a.17; cul2.b-rob1* line was crossed with cv Steptoe and a segregating F2 family was developed. The tightly linked *rob1* marker and a cleaved-amplified polymorphic sequence (CAPS) marker for single-nucleotide polymorphism (SNP) 1_0964 were used to identify 56 homozygous *cul2.b-rob1/cul2.b-rob1* F2 plants (Supplemental Table S1). The *eli-a.17* phenotype of these 56 individuals was determined in F3 families, because the suppressor phenotype is not fully penetrant and some F2 *eli-a.17/eli-a.17; cul2.b-rob1/cul2.b-rob1* plants were uniculm. *eli-a.17* mapped to 2HS 2.2 centimorgan (cM) proximal of SNP 2_0964 at position 17.85 on the SNP map (Supplemental Fig. S4). *eli-a.18* was mapped using the liguleless phenotype in 220 F2 individuals from a cross between Bowman-*eli-a.18; cul2.b-rob1* and cv Harrington. The liguleless trait was mapped 1.6 cM proximal to SNP 3_1284 at position 19.47 on 2HS (Supplemental Fig. S4).

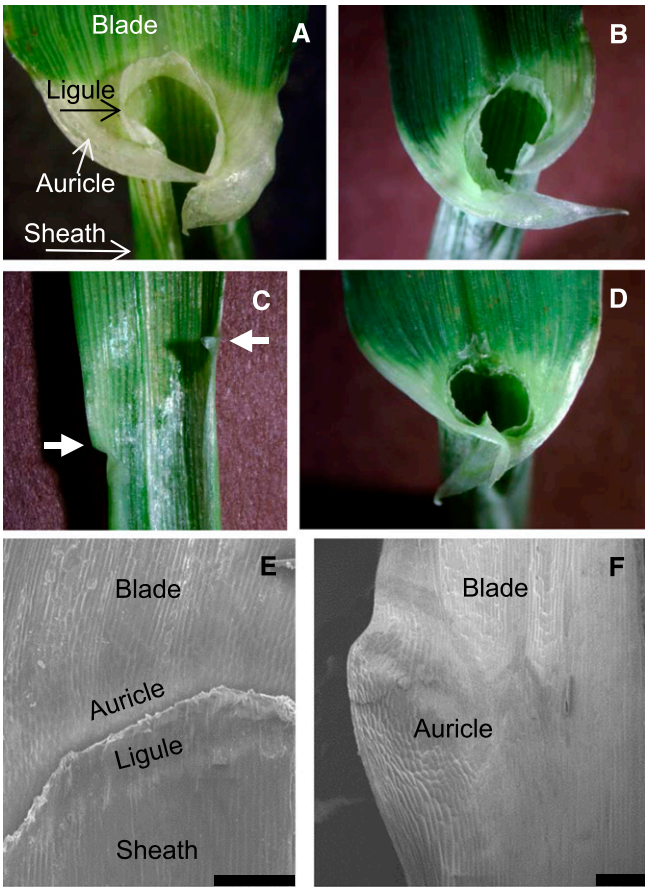

Figure 2. The ligular region in *eli-a* alleles. A to D, Ligules and auricles. A, Nonmutant cv Bowman. B, Bowman-*eli-a.17*. C, Bowman-*eli-a.18*. Note the reduced auricles at the leaf margin, indicated by the arrows and the absence of the ligule. D, Heterozygous Bowman-*eli-a.17/eli-a.18*. Note the reduced ligule and auricle development. E and F, Scanning electron micrographs of the ligular regions. E, Nonmutant cv Bowman. The ligule has been trimmed back to uncover the underlying auricle. F, Bowman-*eli-a.18* ligular region. Bars = 200 μm.

Barley *eli-a* mutants were described previously as recessive mutations producing a phenotype of dwarfed liguleless plants with weak culms that break at the nodes (Lundqvist and Franckowiak, 2002). We observed these characteristics in the *eli-a.18* mutant. In addition, the attachment of outer tillers to the crown was so poor that tillers leaned outward (Fig. 1). These similarities prompted us to test for allelism between *eli-a.18* and the previously described *eli-a* alleles. Six mutants classified as *eligulum* that had been backcrossed into the Bowman background were examined (Druka et al., 2011). Genetic stocks carrying three of the mutations, *eli.12*, *eli-b.5*, and *eli-a.216*, had few of the reported *eli-a* characteristics nor resembled either of our two suppressors and were not pursued. *eli-a.3*, *eli-a.9*, and *eli-a.14* mutant stocks exhibited the short stature and liguleless characteristics of plants carrying the *eli-a.18*

allele. An adult *eli-a.14* plant is shown in Figure 1, and the liguleless trait from *eli-a* plants is shown in Supplemental Figure S3. Three crosses of *eli-a.18* with *eli-a.3*, two crosses with *eli-a.9*, and one cross with *eli-a.14* were made. Ten F1 plants were produced, and they all exhibited short and liguleless mutant phenotypes. An example of the heteroallelic combination *eli-a.9/eli-a.18* is presented in Supplemental Figure S2. These results confirm that our *cul2* suppressors are allelic with *eli-a* mutants.

To determine if *eli-a.3*, *eli-a.9*, and *eli-a.14* suppress the *cul2* uniculm phenotype, we crossed *eli-a.3*, *eli-a.9*, and *eli-a.14* with Bowman-*cul2.b-rob1*. In total, 23 mutant plants were recovered (*eli-a.3/eli-a.3; cul2.b-rob1/cul2.b-rob1*, *eli-a.9/eli-a.9; cul2.b-rob1/cul2.b-rob1*, and *eli-a.14/eli-a.14; cul2.b-rob1/cul2.b-rob1*), and 22 of 23 individuals developed tillers. Examples of the suppression of *cul2.b* by *eli-a.14* and *eli-a.9* are shown in Figure 1 and Supplemental Figure S2. All five *eli-a* alleles tested suppress *cul2*, thereby establishing a role for *ELI-A* in axillary meristem development.

Axillary Bud and Tiller Development in *eli-a* Mutants

To study the impact of *eli-a* on early axillary bud development, we examined 7-d-old shoot apices from Bowman-*eli-a.17; cul2.b-rob1*, Bowman-*cul2.b-rob1*, Bowman-*eli-a.17*, and the nonmutant cv Bowman. Despite being a weak allele, the *eli-a.17* allele was used for this experiment because germination rates were higher and growth more uniform than in other *eli-a* alleles. Two to three primary axillary buds were typically seen in nonmutant cv Bowman seedlings at 7 d (Fig. 3). In these experiments, no axillary buds were seen in *cul2.b* seedlings (Fig. 3), but in previous experiments, occasionally an axillary meristem would develop but would be blocked from forming an axillary bud (Babb and Muehlbauer, 2003). One to two primary axillary buds were present in 7-d-old Bowman-*eli-a.17* seedlings (Fig. 3). In the Bowman-*eli-a.17; cul2.b-rob1* material, zero to two axillary buds were visible at 7 d (Fig. 3). A 7-d-old Bowman-*eli-a.18* shoot apex is shown in Supplemental Figure S5 for comparison.

The rates of axillary bud and tiller development between the *eli-a.17* mutant and the nonmutant were compared, and the numbers of tillers on adult plants for *eli-a.17* were compared with the nonmutant. Developing axillary buds and tillers were counted weekly in dissected seedlings of *eli-a.17* and nonmutant plants at 2 to 6 weeks after planting. Over this period, the rate of axillary bud and tiller emergence was significantly slower in *eli-a.17* plants than in nonmutant plants (Supplemental Fig. S6).

Tiller numbers on field-grown plants were determined for both Bowman-*eli-a.17* and Bowman-*eli-a.18* plants. At maturity, plants carrying the strong mutant allele, *eli-a.18*, had approximately half as many tillers as nonmutant plants, whereas plants carrying the weak *eli-a.17* allele had approximately 20% fewer tillers than

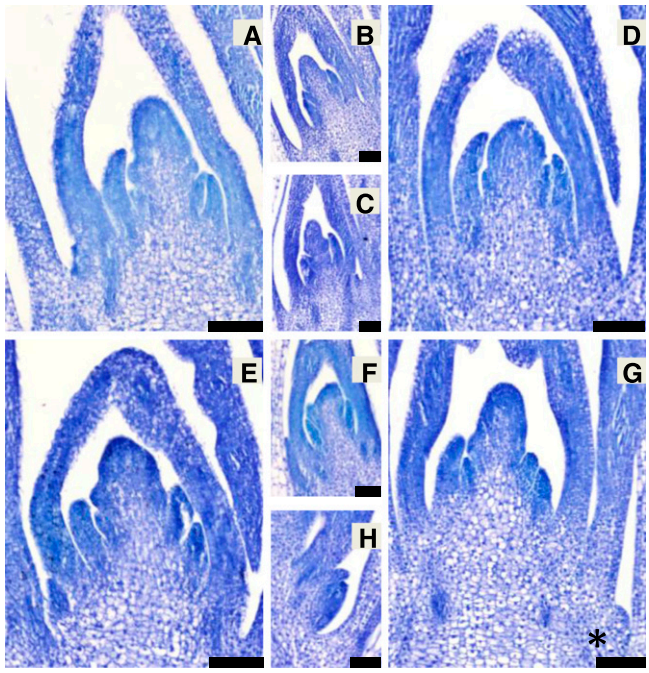

Figure 3. Longitudinal sections of 7-d-old shoot apices from nonmutant and mutant lines stained with Toluidine Blue. Axillary buds are shown in the smaller images, as median sections of the shoot apex generally do not capture the axillary buds. A, Nonmutant cv Bowman shoot apical meristem. B, Cv Bowman axillary bud 3. C, Cv Bowman axillary bud 2. D, Bowman-*cul2.b-rob1* shoot apical meristem. E, Bowman-*eli-a.17* shoot apical meristem. F, Bowman-*eli-a.17* axillary bud. G, Bowman-*eli-a.17; cul2.b-rob1* shoot apical meristem. The edge of a small axillary bud is visible at bottom right (asterisk). H, Section through axillary bud 1 seen in G. Bars = 100 μm.

nonmutant plants (Table I). This small reduction in tillering in *eli-a.17* compared with the nonmutant cv Bowman was consistent with tiller numbers counted from individual families in previous seasons. For example, nonmutant cv Bowman plants had an average of 45.5 (SE = 3.4) tillers per plant and an adjacent family of Bowman-*eli-a.17* plants had 33.9 (SE = 3.41) tillers per plant in the 2013 field. The reduced tiller number in *eli-a.17* and *eli-a.18* mutants compared with the nonmutant and the increase in tiller number in *cul2.b; eli-a* double mutants indicates that the mechanism controlling the rate of tillering and adult tiller number is not necessarily the same mechanism that suppresses the *cul2* mutant phenotype.

Ligule and Auricle Development in *eli-a* Mutants

The grass leaf sheath-blade boundary is marked by two structures, the ligule and the auricle (Fig. 2). The auricle can be divided into two parts, a band of small, light-colored cells separating the blade from the sheath and a flap of tissue growing out from the leaf margin that often wraps around the stem (Fig. 2). The boundary runs perpendicular to the long axis of the leaf, and the

Table I. *Tiller development in* eli-a.17 *and* eli-a.18 *mutants and in nonmutant cv Bowman*
Asterisks indicate $P < 0.05$ by two-tailed Student's *t* test.

Genotype	Tiller Number, 4 Weeks	Tiller Number, 6 Weeks	Tiller Number, Maturity
Cv Bowman[a]	7.69	28.01	33.95
Bowman-*eli-a.17*[a]	6.70	23.93*	27.37*
Cv Bowman[b]	6.61	27.32	43.99
Bowman-*eli-a.18*[b]	4.73	15.75*	21.97*

[a]2015 field. [b]2016 field.

paired auricle flaps are usually directly opposite each other.

Ligules and the bands of auricle cells were generally not visible in *eli-a.18* plants, but small auricle flaps were present (Fig. 2). Figure 2 presents an adaxial view of the ligular region from a nonmutant plant with the ligule cut away to show the underlying auricle cells. A small auricle develops in *eli-a.18* plants at the leaf margin and extends a short distance inward (Fig. 2; Supplemental Fig. S3). Ligules were not obvious in most plants, although small rudimentary ligules have been seen. When present, rudimentary ligules were short and did not span the width of the leaf (Supplemental Fig. S3).

A range of ligule and auricle development was seen in the five *eli-a* alleles. Ligule and auricle development was visibly disrupted in *eli-a.3*, *eli-a.9*, *eli-a.14*, and *eli-a.18* leaves (Supplemental Fig. S3). Ligules and auricles appeared normal in homozygous *eli-a.17* plants (Fig. 2; Supplemental Fig. S3). However, heterozygous *eli-a.17/eli-a.18* plants have small ligules while heterozygous *eli-a.18/ELI-A* plants produce normal ligules, indicating that the *eli-a.17* allele is not equivalent to the nonmutant allele for ligule development (Fig. 2; Supplemental Fig. S3).

Another characteristic of leaf development in *eli-a* mutants was the displacement of the blade-sheath boundary, as indicated by the placement of auricle flaps at the leaf margin (Supplemental Fig. S3). In nonmutant plants, these structures are opposite one another on the leaf, and the blade-sheath boundary runs approximately perpendicular to the longitudinal axis of the leaf (Fig. 2; Supplemental Fig. S3). Displacement of the blade-sheath boundary was commonly observed in *eli-a.3*, *eli-a.9*, *eli-a.14*, and *eli-a.18* (Supplemental Fig. S3). This aberrant boundary positioning was infrequent with nonmutant and *eli-a.17* leaves.

Inflorescence Development

eli-a mutant spikes have a compact appearance with spikelets packed tightly together, particularly toward the tip (Supplemental Fig. S7; Lundqvist and Franckowiak, 2002). This characteristic is less obvious in weaker alleles like *eli-a.3* and *eli-a.17* (Supplemental Fig. S7). The *cul2* mutation produces spikes with spikelets irregularly placed along the spike, particularly near the tip (Babb and Muehlbauer, 2003). The expression of these traits in double mutant *eli-a; cul2.b* plants ranges from compact spikes with an irregular arrangement of spikelets to severe disruption of spikelet formation (Supplemental Fig. S7). Thus, although the *eli-a* mutation partially suppresses the axillary meristem defect in *cul2* mutants, the *cul2* spike phenotype is not suppressed.

Secondary Cell Wall Defects in *eli-a* Mutants

Nonmutant leaves from cv Bowman have midrib, leaf margin, and bundle sheath extension cells with thick secondary cell walls providing strength to the leaves. Stained with Safranin O, these cells appeared small with thick red cell walls (Fig. 4). Corresponding cells in Bowman-*eli-a.18* leaves were larger with thin cell walls (Fig. 4). Safranin O stains lignin, and the weaker staining seen in *eli-a.18* suggests reduced lignin content in *eli-a.18* (Ruzin, 1999). These changes may explain the lack of structural strength and the tendency to droop downward in mutant leaves (Fig. 4). *ELI-A* apparently has a similar function in other tissues. Epidermal cells in the culm and cells immediately under the epidermis have thick cell walls in nonmutant plants (Supplemental Fig. S8). The corresponding cells from *eli-a.18* and *eli-a.3* mutant culms have thin cell walls (Supplemental Fig. S8). This may explain the weakness reported in *eli-a* culms (Lundqvist and Franckowiak, 2002). However, secondary cell walls did develop in the xylem and other cells within vascular bundles in *eli-a.18* mutant plants, demonstrating that *ELI-A* is not an absolute requirement for secondary wall development (Fig. 4).

Disrupting cell wall development may explain other characteristics of *eli-a* mutants. In *eli-a.18* mutant plants, secondary cell wall formation in the mestome sheath and bundle sheath extensions was greatly reduced. Structural strength is but one function of secondary cell walls (for review, see Leegood, 2008). Fricke (2002) proposed that the bundle sheath regulates the flow of water and photosynthate between the leaf mesophyll and the vascular system. Other work suggests that bundle sheath extensions are an adaptation for desiccation stress (Kenzo et al., 2007). Physiological limitations imposed by mutant cell walls could explain the semidwarf stature and reduced rate of tillering in *eli-a* plants but would not account for the suppression of the *cul2* axillary meristem trait. However, cell wall stiffness in the shoot apex influences auxin transport, *CUC3*

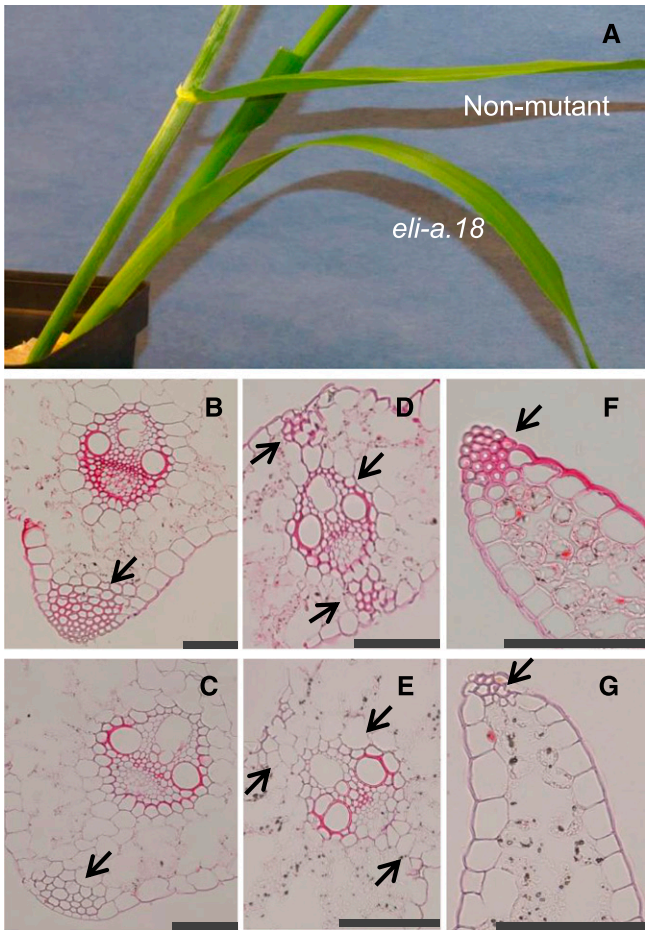

Figure 4. Secondary cell wall development. A, Comparison of leaves from mature nonmutant cv Bowman and Bowman-*eli-a.18* plants. B to G are Safranin O stained. B, Midrib from nonmutant plant. C, Midrib from Bowman-*eli-a.18* plant. D, Leaf vein from nonmutant plant. E, Leaf vein from Bowman-*eli-a.18* plant. F, Leaf margin from nonmutant plant. G, Leaf margin from Bowman-*eli-a.18* plant. Arrows point to cell wall differences in the leaf midrib (B and C), the bundle sheath extension and mestome sheath (D and E), and the leaf margin (F and G). Bars = 100 μm.

expression, and leaf primordia emergence in other systems and provides a plausible mechanism for controlling axillary meristem development (Kierzkowski et al., 2012; Nakayama et al., 2012; Fal et al., 2016).

Isolation and Characterization of the *ELI-A* Gene

The *ELI-A* gene was identified by comparing the transcriptomes of the sodium azide-generated *eli-a.17* and *eli-a.18* mutant alleles against nonmutant plants. RNA was isolated and sequenced from 2-week-old seedling crown tissue from cv Bowman, Bowman-*cul2.b*, Bowman-*cul2.b-rob1*, Bowman-*eli.a-17*, Bowman-*cul2.b-rob1; eli.a-17*, Bowman-*eli-a.18*, and Bowman-*cul2.b-rob1; eli-a.18*. De novo assembly of sequence reads from the cv Bowman line produced 31,976 transcripts (Supplemental Data S1). SNPs were then identified between nonmutant cv Bowman and the mutant lines. These SNPs would include any existing variation in the cv Bowman lines and mutations induced by the sodium azide treatment, including the causative mutations for *eli-a.17* and *eli-a.18* (Supplemental Tables S2–S7). Transcript11292 (Supplemental Data S1) contained an SNP at position 1,103 from the Bowman-*cul2.b-rob1; eli-a.17* and Bowman-*eli.a-17* lines and a different SNP at position 796 in the Bowman-*cul2.b-rob1; eli-a.18* and Bowman-*eli-a.18* lines (Supplemental Tables S2–S5). These two SNPs in Transcript11292 were not present in the cv Bowman, Bowman-*cul2.b-rob1* progenitor line, or the related Bowman-*cul2.b* line, providing evidence that the sequence differences were not preexisting polymorphisms (Supplemental Tables S6 and S7). Both SNPs were confirmed by Sanger sequencing PCR products from the cv Bowman, Bowman-c*ul2.b- rob1; eli-a.17*, and Bowman-*cul2.b-rob1; eli-a.18* genomic DNAs.

A full-length cDNA sequence, AK375036, matching Transcript11292 was identified in a BLASTn search of the GenBank nonredundant sequence database. The entire predicted coding region of AK375036 was sequenced from the *eli-a.17*, *eli-a.18*, *eli-a.3*, *eli-a.9*, and *eli-a.14* alleles (Fig. 5). Cv Foma, the progenitor allele of *eli-a.3* and *eli-a.9*, cv Kristina, the progenitor allele of *eli-a.14*, the Bowman-*cul2.b-rob1* line, progenitor of *eli-a.17* and *eli-a.18*, and the backcross parent cv Bowman also were sequenced. *eli-a.3*, *eli-a.9*, and *eli-a.17* contained the nonconservative amino acid substitutions Pro to Ser, Thr to Ile, and Asp to Tyr, respectively. The *eli-a.14* and *eli-a.18* alleles contained nonsense mutations. This cDNA corresponds to gene model MLOC_58453 from the barley genome (International Barley Genome Sequencing Consortium, 2012).

MLOC_58453 cosegregated with the liguleless phenotype in the *eli-a.18* mutant and the *eli-a.17* suppressor phenotype in the mapping populations described above. MLOC_58453 was mapped in the Bowman-*cul2.b-rob1; eli-a.18* cv Harrington F2 population using a CAPS marker targeting the mutated base pair (Supplemental Table S1). As expected, all liguleless plants were homozygous for the mutant MLOC_58453 CAPS allele (Supplemental Fig. S4). Similarly, an SNP located within the MLOC_58453 coding region cosegregated with the suppressor phenotype in the *eli-a.17* mapping population (Supplemental Fig. S4; Supplemental Table S1). MLOC_58453 has been mapped to chromosome 2HS on the barley genome assembly (International Barley Genome Sequencing Consortium, 2012).

ELI-A Is a Conserved Plant Gene Containing an RNaseH-Like Domain

Homologous *ELI-A* sequences were found in land plants ranging from Arabidopsis and rice to the nonvascular and primitive vascular plants *Physcomitrella*

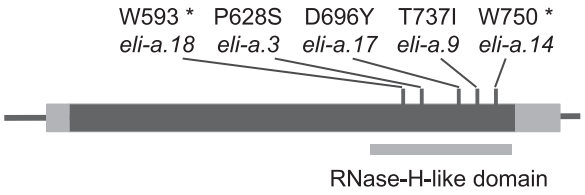

Figure 5. The *ELI-A* gene and locations of mutations. The dark gray box indicates the single exon in the gene, and lighter gray boxes mark the 5′ and 3′ untranslated regions. Mutations in *eli-a.14* and *eli-a.18* created stop codons. Prediction programs Phyre[2], LOMETS, and InterProScan 5 identified an RNaseH-like domain at the C-terminal end of the peptide.

patens and *Selaginella moellendorffii* (Supplemental Table S8). A distantly related sequence was present in the green alga *Chlamydomonas reinhardtii*. Mutant phenotypes in Arabidopsis have not been reported in TAIR, and the two homologs, AT1G12380 and AT1G62870, are described as hypothetical proteins (https://www.arabidopsis.org/, May 2017), nor are the maize gene models homologous with *ELI-A* associated with a maize phenotype or classical gene (http://maizegdb.org/, May 2017). A phylogenetic tree developed from these sequences is presented in Supplemental Figure S9 (Dreeper et al., 2008). Despite the sequence conservation, there is a lack of evidence for *ELI-A* function outside of barley.

We examined peptide sequences of the barley ELI-A protein and in homologous rice and Arabidopsis proteins. The peptides from barley, rice, and Arabidopsis were predicted by Phyre[2], LOMETS, and InterProScan 5 to contain an RNaseH-like domain (Quevillon et al., 2005; Wu and Zhang, 2007; Kelley and Sternberg, 2009). InterProScan 5 did provide additional details, but Phyre[2] and LOMETS identified the putative RNaseH-like domain as a member of the Hermes transposase class. The Hermes class of RNaseH-like domains is found in hAT family transposons; hAT family transposons also contain an N-terminal BED-type zinc finger and the hAT domain (Hickman et al., 2005).

Further examination of the relationship of the ELI-A protein to members of the RNaseH-like superfamily found that the Hermes domain is a class I RNaseH that is within clade B under the classification scheme of Majorek et al. (2014). This family is composed mainly of transposases with endonuclease activity, although one member of clade B encodes the human P52^{rIPK} protein that regulates a human RNA-dependent Ser/Thr protein kinase (Gale et al., 2002). Phyre[2] detected BED-type zinc fingers in the rice and Arabidopsis peptides with moderate confidence. However, the hAT domain was not detected by Phyre[2], LOMETS, or InterProScan 5 in barley, rice, or Arabidopsis. At present, the origin of *ELI-A* from a transposon is not known.

ELI-A Expression Pattern

The expression levels of *ELI-A* from eight tissues were calculated from previously published RNA sequencing (RNAseq) data (International Barley Genome Sequencing Consortium, 2012). At this level of resolution, expression was highest in 5- and 15-mm-long immature inflorescences (Supplemental Fig. S10). *ELI-A* expression levels were low in most other tissues. RNA was extracted from axillary buds, 5-mm-long inflorescences, and leaf blades for quantitative reverse transcription PCR (RT-qPCR) to validate the RNAseq data. Transcript levels were highest in the inflorescence, while transcript levels were below the threshold of detection in leaf tissue, consistent with results from the RNAseq data (Supplemental Fig. S10).

RNA in situ hybridizations were performed to further refine the distribution of *ELI-A* transcripts. In nonmutant, 4-d-old shoot apices, expression was strong in leaf midribs, along the leaf margin, in the bundle sheath surrounding vascular bundles, and in bundle sheath extension cells (Fig. 6). A sense control is shown in Supplemental Figure S11. *ELI-A* transcripts were detected in similar locations in *cul2.b* mutant seedlings (Fig. 6). In transverse *cul2.b* sections, expression was detected in small clusters of cells along the abaxial leaf surface (Fig. 6). Expression at this location was variable and also was seen in nonmutant plants (Supplemental Fig. S11). There were no consistent differences in expression between nonmutant and *cul2.b* plants.

ELI-A transcripts are present in developing ligules. A low level of *ELI-A* transcripts was found in emerging ligules (Fig. 6; Supplemental Fig. S11) but not in older ligules (Fig. 6). In younger leaf primordia, a prominent signal was present slightly above the base of leaf primordia on the adaxial side in longitudinal sections. This signal appeared to correspond to the band of expression found on the adaxial surface of leaf primordia in transverse sections (Fig. 6). A serial section from higher up along this shoot apex showed expression continuing along the adaxial surface (Supplemental Fig. S11). This is the expected location of the preligule band, which marks the boundary between the blade and sheath. To verify this, we looked at the expression of the barley homolog of the maize *Liguleless1* (*Lg1*) gene. The maize *Lg1* gene is expressed at the preligule band at the blade-sheath boundary (Moon et al., 2013). *ELI-A* and *HvLG1* transcripts were both found on the adaxial surface of the blade-sheath boundary in serial sections from the same shoot apex (Fig. 6). An *HvLG1* sense control is shown in Supplemental Figure S11. Taken together, these results indicate that *ELI-A* acts like a boundary gene in the development of the blade-sheath boundary.

Weak staining was sometimes seen in axillary buds and in leaf axils adjacent to developing axillary meristems as well as within axillary buds in longitudinal sections (Fig. 6; Supplemental Fig. S11). In transverse sections, this transcript appeared to associate with developing vascular bundles rather than the leaf axil or axillary meristem (Fig. 6). *ELI-A* expression farther down the shoot apex where the axillary bud emerged from the shoot apex was very weak compared with expression around vascular bundles higher up the shoot apex (Supplemental Fig. S11). The expression

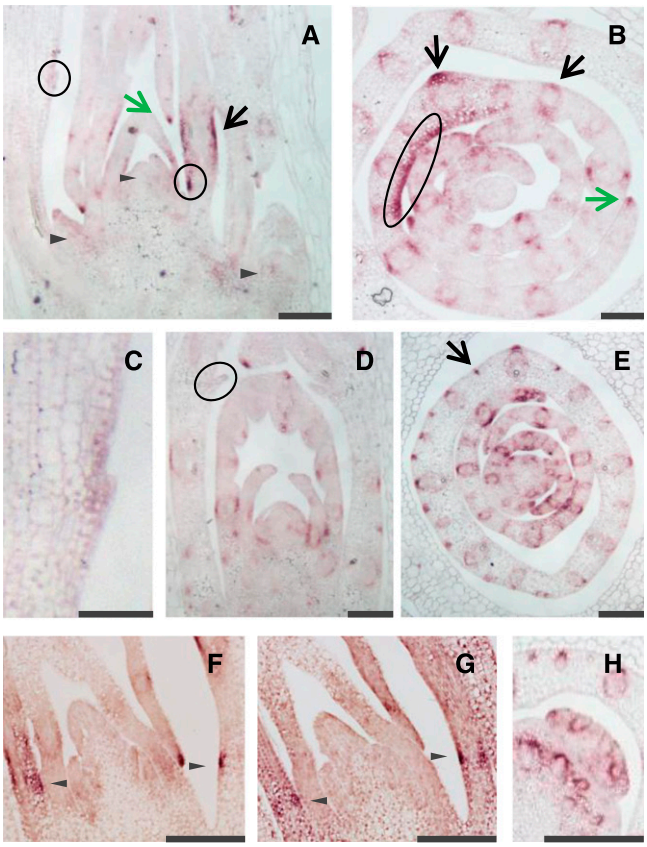

Figure 6. *ELI-A* expression in nonmutant and *cul2.b* seedlings. A to C, Four-day-old nonmutant shoot apex probed with an antisense *ELI-A* probe. A, Longitudinal section showing little staining in or adjacent to the shoot apical meristem and axillary buds, indicated by triangles. Short patches of staining at the adaxial and abaxial sides of leaves were seen occasionally (black arrow); this pattern is likely from vascular bundles, as seen in B and H. Staining was observed in newly forming ligules and leaf primordia that may represent developing ligules (circled). Leaf margins also were stained (green arrow). B, Transverse section showing staining in leaf margins, midribs, and around vascular bundles. Staining along a portion of the adaxial side of a developing leaf (circled) can be followed across the leaf in serial sections and may be associated with the developing ligules. C, Closeup view of the ligule circled in A. D and E, Four-day-old *cul2.b* shoot apex probed with an antisense *ELI-A* probe. D, Longitudinal section of a *cul2.b* shoot. E, Transverse section of a *cul2.b* shoot. The *ELI-A* staining pattern was similar to that of nonmutant shoot apices. The variable staining in small clusters of cells along the abaxial leaf surface (arrow) was seen in nonmutant plants (Supplemental Fig. S11); transcripts were not detected in the older ligules (circled). F and G, Serial sections of 4-d-old shoots probed for *ELI-A* or *HvLg1*. F, *ELI-A* staining was observed in the same location as the adaxial *HvLg1* staining. G, *HvLg1* staining was detected on the adaxial and abaxial surfaces. H, *ELI-A* expression in leaf axils and axillary buds is associated with vascular bundles. Bars = 100 μm in C and 200 μm in other images.

pattern of *ELI-A* did not indicate a direct function in boundary formation or stem cell maintenance.

Sclerenchyma cells are found in developing leaf ribs, hypodermal sclerenchyma cells, and leaf margins from barley plants (Wenzel et al., 1997; Trivett and Evert, 1998). These are locations where *ELI-A* transcripts were detected in leaf primordia. In *eli-a.18* mutants, cells comprising midribs have thin cell walls and lack the thick secondary cell walls of normal rib cells. Elsewhere in the leaf and in the culm, *ELI-A* transcripts coincided with cells having thickened secondary cell walls (Figs. 5 and 6). *ELI-A* transcripts were not detected in the xylem or phloem (Fig. 6; Supplemental Fig. S11). This absence of secondary cell walls can explain the weak leaves and culms in *eli-a* mutant plants. However, the absence of *ELI-A* transcripts in leaf axils from both *CUL2* and *cul2.b* plants argues against a direct role for secondary cell walls in the suppression of the *cul2* tillering phenotype by *eli-a*.

ELI-A Acts Like a Boundary Gene in the Leaf But Not in the Leaf Axil

A conserved set of genes are believed to control leaf and axillary meristem development. In tomato and other eudicots, the development of leaf serrations, leaflets, and axillary meristems in leaf axils is regulated by *CUC*, *RAX*, and *LATERAL SUPPRESSOR* (Busch et al., 2011). Grass leaves lack the serrated margins and leaflets common in eudicots, but there is a boundary between the blade and sheath consisting of the ligule and auricles (Langdale, 2005; Lewis and Hake, 2016). Laser microdissection transcriptome analysis showed maize *CUC2*, *BOP* (homologous to barley CUL4), and *ELI-A* homologs up-regulated at the blade-sheath boundary (Johnston et al., 2014). In situ hybridizations confirmed the maize *CUC2* and *BOP* expression in newly forming ligules at the leaf blade-sheath and lateral organ initiation boundaries including axillary meristems (Johnston et al., 2014). This postulated genetic system may derive from a common evolutionary origin for leaves and axillary meristems, as suggested by Busch and colleagues (2011), and is consistent with expectations from the barley phytomer model proposed by Forster and coworkers (2007). Alternatively, the conserved genes may be part of a conserved genetic module that acts in leaf and axillary meristem development (Carroll, 2008).

This system of genes is expected to function in barley development. The barley *BOP* homolog, *CUL4*, is expressed in newly formed ligules at the blade-sheath junction and at axillary meristem boundaries in leaf axils (Tavakol et al., 2015). However, *CUL4* is expressed in developing ligules and does not appear to specify the location of the blade-sheath boundary (Tavakol et al., 2015). Like *CUL4*, *ELI-A* is expressed in newly forming ligules but also is expressed earlier in development than *CUL4*, where its expression pattern overlaps the barley homolog of the maize *Lg1* gene in the preligular region separating the blade from the sheath (Moon et al., 2013). In addition, the *ELI-A* mutants (*eli-a.9*, *eli-a.3*, *eli-a.14*, and *eli-a.18*) exhibiting a liguleless phenotype also exhibit a disrupted blade-sheath boundary (Supplemental Fig. S3). Taken together, our results

show that *ELI-A* and *CUL4* are both necessary to produce a ligule, with *ELI-A* acting at a similar time and place with *HvLg1* to establish the leaf blade-sheath boundary.

CUL4 and *ELI-A* both have roles in axillary meristem development. However, their roles in axillary development appear different because the *cul4* and *eli-a* tillering phenotypes share few characteristics. The *cul4* mutation restricts axillary meristem development to a short developmental window; new axillary buds cease appearing after 3 to 4 weeks in *cul4.5* plants (Tavakol et al., 2015). The *eli-a* mutation slows the rate of axillary meristem development. Furthermore, *eli-a* mutants suppress the low-tillering *cul2* phenotype; *cul4* does not (Babb and Muehlbauer, 2003).

RNA in situ hybridization provided further evidence for differing roles for *ELI-A* during leaf and axillary branch development. The *ELI-A* transcripts were present at the leaf blade-sheath boundary, where it participates in ligule development. Although *ELI-A* transcripts were occasionally detected in or adjacent to developing axillary buds in longitudinal sections, *ELI-A* was shown in transverse sections to be closely associated with vascular bundles rather than organ boundaries or meristematic regions. This expression pattern in the leaf axil was not similar to that of other characterized axillary meristem boundary genes, including *CUL4* and the rice *CUC3* and *RA2* homologs (Oikawa and Kyozuka, 2009; Tavakol et al., 2015). It is possible that transient *ELI-A* expression in axillary meristems or organ boundaries was not detected or that the *ELI-A* protein is transported, as shown for the rice *LAX* protein (Oikawa and Kyozuka, 2009). While acknowledging these possibilities, our data support a model where *ELI-A* has an early role and *CUL4* has a later role in creating the blade-sheath boundary during leaf development. However, during axillary meristem development, *CUL4* is expressed in the leaf axil and plays a role in boundary formation. While *ELI-A* does not appear to be expressed in the leaf axil boundary, it still has a role in axillary meristem development. Taking these findings together, we propose that *ELI-A* acts like a boundary gene at the leaf blade-sheath boundary and promotes secondary cell wall formation in leaves and other tissues but acts in an unknown manner during axillary meristem development.

MATERIALS AND METHODS

Plant Materials and Populations

Barley (*Hordeum vulgare*) mutant alleles *cul2.b*, *eli-a.3*, *eli-a.9*, *eli-a.14*, and *rob1* were obtained from the collection of mutants backcrossed to cv Bowman (Druka et al., 2011). Plants were either field grown or grown under controlled conditions in a greenhouse or growth chamber with 16 h of light at 22°C and 8 h dark at 18°C. Supplemental Table S9 provides information on the mutant alleles and barley cultivars used here.

The *cul2* suppressor screen was conducted by mutagenizing Bowman-*cul2.b-rob1* grain. The *rob1* allele is approximately 2 cM from *cul2* and produces an orange lemma phenotype that was used to track the tightly linked *cul2.b* allele. Approximately 20,000 Bowman-*cul2.b-rob1* kernels were treated with sodium azide according to the protocol described by Döring et al. (1999). From the M2 plants, over 15,000 M3 families (~70,000 plants) were produced and screened. M3 families segregating for plants with tillers were identified. Families were retested for the suppressor phenotype in subsequent generations.

To recover homozygous *eli-a.17* plants, we conducted a single backcross of *eli-a.17/eli-a.17; cul2.b-rob1/cul2.b-rob1* plants to the nonmutant cv Bowman and self-pollinated an F1 plant to generate an F2 population. Families derived from phenotypically nonmutant F2 plants were screened in the F3 and F4 generations to recover homozygous *eli-a.17/eli-a.17* and *eli-a.17/eli-a.17; cul2.b-rob1/cul2.b-rob1* lines (Supplemental Fig. S12). *eli-a.18* mutant plants were identified by their short stature and liguleless leaves. F2 populations segregating *eli-a.17* and *eli-a.18* were produced by crossing the Bowman-*eli-a.18; cul2.b-rob1* line with the nonmutant cv Harrington and by crossing the Bowman-*eli-a.17; cul2.b-rob1* line with the nonmutant cv Steptoe.

Seedling tests for the suppression of *cul2.b* by *eli-a.3*, *eli-a.9*, and *eli-a.14* were performed by crossing the mutants and recovering *eli-a/+; cul2.b/cul2.b* individuals. These plants were allowed to self-pollinate. Tillering phenotypes of suppression of *cul2* by *eli-a.3* and *eli-a.14* were scored in the growth chamber in 3- to 4-week-old F2 plants. The suppression of *cul2.b* by *eli-a.9* was tested in field-grown F2 families.

Morphological Characterization

Shoot apices from 1-week-old seedlings were sectioned and stained to examine axillary bud development as described previously (Babb and Muehlbauer, 2003). Axillary buds and tillers were counted on growth chamber-grown plants in weeks 2 through 6. Three replicates, three plants per replication, were counted at each time point; at least eight plants were examined in all but two time points. Leaves were removed to count axillary buds and tillers. Axillary buds were further classified as primary axillary buds, those growing in leaf axils, and secondary axillary buds, those growing in tiller axils (Dabbert et al., 2010). Tiller number was determined from field-grown plants at 4 weeks, 6 weeks, and maturity; five plants per replicate with six replicates of nonmutant and Bowman-*eli-a.17*, and five replicates of Bowman-*eli-a.18*, were randomized in the field.

Ligular regions were examined on 4- to 6-week-old plants grown in the growth chamber or greenhouse. The development of ligules, auricles, and other features was characterized from the second or third leaf. The leaf blade-sheath junction region was photographed under low-power light microscopy and with cryo-scanning electron microscopy. Scanning electron microscopy was performed on a Hitachi S3500N scanning electron microscope at 5 or 10 kV (Ahlstrand, 1996).

For histological work, plant tissues were fixed in paraformaldehyde and embedded in paraffin (Javelle et al., 2011). Sections were stained with Toluidine Blue or Safranin O (Humason, 1979; Ruzin, 1999). RNA in situ hybridizations were performed as described by Javelle et al, (2011). Probes for RNA in situ hybridizations were developed from PCR amplicons from genomic DNA using primers ELI-1393F and ELI-1877R or HvLG1-79F and HvLG1-598R and then cloned into pGEM-T Easy (Promega). Plasmids were used as templates for PCR with M13 forward and reverse primers. RNA was synthesized from the resulting amplicons with SP6 or T7 RNA polymerase to make the sense and antisense probes using the Roche DIG RNA Labeling Kit (Sigma-Aldrich).

Molecular Biology Procedures

Procedures for DNA isolation, PCR, CAPS markers, and other routine molecular techniques were described previously (Dabbert et al., 2010). PCR primers (Supplemental Table S10) were developed using the program Primer3 (Rozen and Skaletsky, 2000). Sanger sequencing was performed by the University of Minnesota Genomics Center. CAPS markers were developed from previously mapped SNP sequences (Close et al., 2009), and the program JoinMap 4 was used to calculate map distances (Van Ooijen, 2006).

Total RNA for sequencing (RNAseq) was isolated from crown tissue containing the shoot apical meristem and axillary meristems from 14-d-old seedlings grown in growth chambers using the RNeasy Plant Mini Kit (Qiagen). There were three replicates of each genotype (cv Bowman, Bowman-*cul2.b*, Bowman-*cul2.b-rob1*, Bowman-*eli.a-17*, Bowman-*cul2.b-rob1; eli.a-17*, Bowman-*eli-a.18*, and Bowman-*cul2.b-rob1; eli-a.18*), six seedlings per replicate, and tissue from each genotype was pooled. Poly(A^+) RNA isolation, library construction, and Illumina sequencing were performed by the University of Minnesota Genomics Center. Fragment sizes for sequencing averaged 200 bp, after accounting for adaptor sequences, and 76-bp paired-end reads were produced.

Relative *ELI-A* expression levels were compared in inflorescence, axillary bud, and leaf blade tissues by RT-qPCR using the procedure described by Tavakol et al. (2015). Total RNA was isolated from 1-cm-long axillary buds from 2-week-old seedlings, 5-mm-long inflorescences, and leaf blades from 4-week-old seedlings using the RNeasy Kit (Qiagen). Approximately 250 ng of total RNA was DNase treated (RQ1 RNase-Free DNase; Promega) prior to cDNA synthesis with the ImProm-II Reverse Transcription System (Promega). One-third of the product was used for PCR. Quantitative PCR was performed on the Applied Biosystems StepOnePlus Real Time PCR System with the QuantiFast SYBR Green mix (Qiagen). *GAPDH* and *UBI* were used for normalization (Tavakol et al., 2015). Three replicates, with three to five plants each, were randomized and grown together in a growth chamber as described above. Primer sequences are shown in Supplemental Table S10.

Sequence Assembly Pipeline and SNP Analysis

Reads for all samples were quality trimmed from both ends with custom Java code using a base quality cutoff of Phred 20. Reads shorter than 30 bp were discarded. Trimmed reads from the cv Bowman sample were assembled de novo using the Trinity transcriptome assembler on default settings (release r2011-05-13; Grabherr et al., 2011). This resulted in a total of 31,976 transcript sequences (Supplemental Data S1).

Trimmed reads from each mutant sample were mapped separately to the Bowman Trinity transcripts using the Bowtie read mapper version 0.12.7 (Langmead et al., 2009). To keep mismapping and the resulting false-positive SNPs to a minimum, a strict mismatch rate of one mismatch per read was applied. Reads were mapped in all mode, which allows multimappable reads to map to all of their possible mapping locations. The –best –strata parameter was used to ensure that only the best mapping locations were reported.

For each genotype, SNP discovery was carried out using custom-written code implemented as a prototype feature in Tablet (Milne et al., 2013). The raw variant data were then filtered using a minor allele frequency of 0.9 or greater to identify homozygous SNPs with the cv Bowman reference sequence only. Several further stages of SNP filtering followed, all of which were aimed at removing false-positive SNPs. First, SNPs that were less than one read's length from the contig start or end, or regions with zero read coverage, were removed, as a large proportion of these can be assumed to be artifacts caused by misassembly of the reference sequence (M. Bayer, unpublished data). SNPs with fewer than six instances of the alternate allele also were removed to exclude low-coverage, low-confidence variants. We called SNPs by mapping the cv Bowman reads against the cv Bowman Trinity assembly as a control set, on the assumption that any SNPs found in this largely homozygous cultivar must be artifacts caused by read mismapping or misassembly of the reference sequence. SNPs discovered in this data set were subsequently removed from all of the mutant SNP sets. The remaining robust SNPs were used for analysis.

Accession Numbers

RNAseq data have been deposited into the National Center for Biotechnology Information Short Read Archive with accession number SRP076379. *ELI-A* sequences were deposited in the National Center for Biotechnology Information database with accession numbers KU844110 to KU844117. Additional sequences mentioned in this article can be found in the GenBank, TAIR, or PlantGDB databases under the following accession numbers: GenBank/EMBL, Bradi5g04710 (XM_003581043), Bradi5g04720 (XM_003579296), CHLREDRAFT_180901 (XM_001692084), LOC_Os04g19140 (XM_015779144), LOC_Os02g25230 (XM_015767599), PP1S21_302V6 (XM_001756068), PP1S105_108V6 (XM_001768660), PP1S226_73V6 (XM_001777733), PP1S111_138V6 (XM_001769128), SELMODRAFT_231485 (XM_002969799), SELMODRAFT_10589 (XM_002985134), Si009424m.g (XM_004975201), Si016308m.g (XP_004952406), Sb04g014800 (XM_002453721), Solyc08g079550 (XM_004246091), Solyc03g007180 (XM_004234118), Zm00001d004164 (XR_562337), Zm00001d025091 (XM_008664864), Zm00001d015889 (XM_008647228), and Zm00001d053254 (XM_008681506); PlantGDB, Sb06g003790.1; and TAIR, AT1G12380 and AT1G62870. Original photographs used for the figures have been archived at the University of Minnesota Data Repository and can be accessed at https://doi.org/10.13020/D61H4D.

Supplemental Data

The following supplemental materials are available.

Supplemental Figure S1. Suppression of *cul2* by *eli-a.17* and *eli-a.18* promotes tillering.

Supplemental Figure S2. Genetic testing of *eli-a* alleles.

Supplemental Figure S3. Ligule development in *eli-a* alleles.

Supplemental Figure S4. Mapping *eli-a.17* and *eli-a.18* on chromosome 2HS.

Supplemental Figure S5. Axillary bud development in Bowman-*eli-a.18*.

Supplemental Figure S6. Rate of axillary bud and tiller appearance.

Supplemental Figure S7. *eli-a* spike phenotypes.

Supplemental Figure S8. Secondary cell wall development in culms.

Supplemental Figure S9. Phylogenetic tree of *ELI-A* homologs.

Supplemental Figure S10. *ELI-A* expression data.

Supplemental Figure S11. *ELI-A* in situ hybridizations.

Supplemental Figure S12. Crossing scheme to develop *eli-a.17* and Bowman-*cul2.b-rob1; eli-a.17* families.

Supplemental Table S1. CAPS markers for *eli-a* alleles and mapping.

Supplemental Table S2. *eli-a.17; cul2.b-rob1* SNP list.

Supplemental Table S3. *eli-a.18; cul2.b-rob1* SNP list.

Supplemental Table S4. *eli-a.17* SNP list.

Supplemental Table S5. *eli-a.18* SNP list.

Supplemental Table S6. *cul2.b-rob1* SNP list.

Supplemental Table S7. *cul2.b* SNP list.

Supplemental Table S8. Homologous *ELI-A* sequences in other species.

Supplemental Table S9. Plant materials.

Supplemental Table S10. PCR primer sequences.

Supplemental Data S1. RNAseq transcript list.

ACKNOWLEDGMENTS

We thank Bruna Bucciarelli for assistance with microscopy, Lin Li and Juan Gutierrez-Gonzalez for help with bioinformatics, Kevin Smith for providing field space, and Jerome Franckowiak for insights on the interpretation of mutants (Department of Agronomy and Plant Genetics, University of Minnesota); Gail Celio and Grant Barthel for help with scanning electron and light microscopy (University Imaging Center, University of Minnesota); Sue Miller for assistance with RT-qPCR (USDA-ARS); and for providing materials, the Nordic Genetic Resource Center, Harold Bockelman (U.S. Department of Agriculture National Small Grains Collection), and Andris Kleinhofs (Washington State University).

Received October 10, 2017; accepted January 28, 2018; published February 12, 2018.

LITERATURE CITED

Ahlstrand GG (1996) Low-temperature low-voltage scanning microscopy (LTLVSEM) of uncoated frozen biological materials: a simple alternative. *In* G Bailey, J Corbett, R Dimlich, J Michael, N Zaluzec, eds, Proceedings of Microscopy Microanalysis. San Francisco Press, San Francisco, pp 918–919

Babb S, Muehlbauer GJ (2003) Genetic and morphological characterization of the barley *uniculm2* (*cul2*) mutant. Theor Appl Genet **106:** 846–857

Bar M, Ori N (2014) Leaf development and morphogenesis. Development **141:** 4219–4230

Becraft PW, Bongard-Pierce DK, Sylvester AW, Poethig RS, Freeling M (1990) The *liguleless-1* gene acts tissue specifically in maize leaf development. Dev Biol **141:** 220–232

Berger Y, Harpaz-Saad S, Brand A, Melnik H, Sirding N, Alvarez JP, Zinder M, Samach A, Eshed Y, Ori N (2009) The NAC-domain transcription factor GOBLET specifies leaflet boundaries in compound tomato leaves. Development **136:** 823–832

Bilsborough GD, Runions A, Barkoulas M, Jenkins HW, Hasson A, Galinha C, Laufs P, Hay A, Prusinkiewicz P, Tsiantis M (2011) Model for the regulation of Arabidopsis thaliana leaf margin development. Proc Natl Acad Sci USA **108:** 3424–3429

Busch BL, Schmitz G, Rossmann S, Piron F, Ding J, Bendahmane A, Theres K (2011) Shoot branching and leaf dissection in tomato are regulated by homologous gene modules. Plant Cell **23:** 3595–3609

Carroll SB (2008) Evo-devo and an expanding evolutionary synthesis: a genetic theory of morphological evolution. Cell **134:** 25–36

Close TJ, Bhat PR, Lonardi S, Wu Y, Rostoks N, Ramsay L, Druka A, Stein N, Svensson JT, Wanamaker S, et al (2009) Development and implementation of high-throughput SNP genotyping in barley. BMC Genomics **10:** 582

Dabbert T, Okagaki RJ, Cho S, Heinen S, Boddu J, Muehlbauer GJ (2010) The genetics of barley low-tillering mutants: *low number of tillers-1* (*lnt1*). Theor Appl Genet **121:** 705–715

Dereeper A, Guignon V, Blanc G, Audic S, Buffet S, Chevenet F, Dufayard JF, Guindon S, Lefort V, Lescot M, et al (2008) Phylogeny.fr: robust phylogenetic analysis for the non-specialist. Nucleic Acids Res **36:** W465–W469

Döring HP, Lin J, Urig H, Salamini F (1999) Clonal analysis of the development of the barley (*Hordeum vulgare* L.) leaf using periclinal chlorophyll chimeras. Planta **207:** 335–342

Druka A, Franckowiak J, Lundqvist U, Bonar N, Alexander J, Houston K, Radovic S, Shahinnia F, Vendramin V, Morgante M, et al (2011) Genetic dissection of barley morphology and development. Plant Physiol **155:** 617–627

Fal K, Landrein B, Hamant O (2016) Interplay between miRNA regulation and mechanical stress for CUC gene expression at the shoot apical meristem. Plant Signal Behav **11:** e1127497

Forster BP, Franckowiak JD, Lundqvist U, Lyon J, Pitkethly I, Thomas WTB (2007) The barley phytomer. Ann Bot **100:** 725–733

Franckowiak JD, Konishi T, Lundqvist U (1997) BGS 254, Orange lemma, rob. Barley Genet Newsl **26:** 235–236

Fricke W (2002) Biophysical limitation of cell elongation in cereal leaves. Ann Bot **90:** 157–167

Gale M Jr, Blakely CM, Darveau A, Romano PR, Korth MJ, Katze MG (2002) $P52^{rIPK}$ regulates the molecular cochaperone $P58^{IPK}$ to mediate control of the RNA-dependent protein kinase in response to cytoplasmic stress. Biochemistry **41:** 11878–11887

Gallavotti A, Zhao Q, Kyozuka J, Meeley RB, Ritter MK, Doebley JF, Pè ME, Schmidt RJ (2004) The role of *barren stalk1* in the architecture of maize. Nature **432:** 630–635

Grabherr MG, Haas BJ, Yassour M, Levin JZ, Thompson DA, Amit I, Adiconis X, Fan L, Raychowdhury R, Zeng Q, et al (2011) Full-length transcriptome assembly from RNA-Seq data without a reference genome. Nat Biotechnol **29:** 644–652

Ha CM, Jun JH, Nam HG, Fletcher JC (2007) *BLADE-ON-PETIOLE 1* and *2* control *Arabidopsis* lateral organ fate through regulation of LOB domain and adaxial-abaxial polarity genes. Plant Cell **19:** 1809–1825

Hepworth SR, Pautot VA (2015) Beyond the divide: boundaries for patterning and stem cell regulation in plants. Front Plant Sci **6:** 1052

Hickman AB, Perez ZN, Zhou L, Musingarimi P, Ghirlando R, Hinshaw JE, Craig NL, Dyda F (2005) Molecular architecture of a eukaryotic DNA transposase. Nat Struct Mol Biol **12:** 715–721

Humason GL (1979) Animal Tissue Techniques, Ed 4. WH Freeman, San Francisco

International Barley Genome Sequencing Consortium (2012) A physical, genetic and functional sequence assembly of the barley genome. Nature **491:** 711–716

Javelle M, Marco CF, Timmermans M (2011) *In situ* hybridization for the precise localization of transcripts in plants. J Vis Exp **57:** e3328

Johnston R, Wang M, Sun Q, Sylvester AW, Hake S, Scanlon MJ (2014) Transcriptomic analyses indicate that maize ligule development recapitulates gene expression patterns that occur during lateral organ initiation. Plant Cell **26:** 4718–4732

Keller T, Abbott J, Moritz T, Doerner P (2006) *Arabidopsis REGULATOR OF AXILLARY MERISTEMS1* controls a leaf axil stem cell niche and modulates vegetative development. Plant Cell **18:** 598–611

Kelley LA, Sternberg MJE (2009) Protein structure prediction on the Web: a case study using the Phyre server. Nat Protoc **4:** 363–371

Kenzo T, Ichie T, Watanabe Y, Hiromi T (2007) Ecological distribution of homobaric and heterobaric leaves in tree species of Malaysian lowland tropical rainforest. Am J Bot **94:** 764–775

Kierzkowski D, Nakayama N, Routier-Kierzkowska AL, Weber A, Bayer E, Schorderet M, Reinhardt D, Kuhlemeier C, Smith RS (2012) Elastic domains regulate growth and organogenesis in the plant shoot apical meristem. Science **335:** 1096–1099

Komatsu K, Maekawa M, Ujiie S, Satake Y, Furutani I, Okamoto H, Shimamoto K, Kyozuka J (2003) LAX and SPA: major regulators of shoot branching in rice. Proc Natl Acad Sci USA **100:** 11765–11770

Langdale JA (2005) The then and now of maize leaf development. Maydica **50:** 459–467

Langmead B, Trapnell C, Pop M, Salzberg SL (2009) Ultrafast and memory-efficient alignment of short DNA sequences to the human genome. Genome Biol **10:** R25

Lee DK, Geisler M, Springer PS (2009) *LATERAL ORGAN FUSION1* and *LATERAL ORGAN FUSION2* function in lateral organ separation and axillary meristem formation in Arabidopsis. Development **136:** 2423–2432

Leegood RC (2008) Roles of the bundle sheath cells in leaves of C_3 plants. J Exp Bot **59:** 1663–1673

Lewis MW, Hake S (2016) Keep on growing: building and patterning leaves in the grasses. Curr Opin Plant Biol **29:** 80–86

Lundqvist U, Franckowiak JD (2002) BGS 623, Eligulum-a, eli-a. Barley Genet Newsl **32:** 124

Majorek KA, Dunin-Horkawicz S, Steczkiewicz K, Muszewska A, Nowotny M, Ginalski K, Bujnicki JM (2014) The RNase H-like superfamily: new members, comparative structural analysis and evolutionary classification. Nucleic Acids Res **42:** 4160–4179

Mathan J, Bhattacharya J, Ranjan A (2016) Enhancing crop yield by optimizing plant developmental features. Development **143:** 3283–3294

Milne I, Stephen G, Bayer M, Cock PJ, Pritchard L, Cardle L, Shaw PD, Marshall D (2013) Using Tablet for visual exploration of second-generation sequencing data. Brief Bioinform **14:** 193–202

Moon J, Candela H, Hake S (2013) The Liguleless narrow mutation affects proximal-distal signaling and leaf growth. Development **140:** 405–412

Müller D, Schmitz G, Theres K (2006) Blind homologous R2R3 Myb genes control the pattern of lateral meristem initiation in *Arabidopsis*. Plant Cell **18:** 586–597

Nakayama N, Smith RS, Mandel T, Robinson S, Kimura S, Boudaoud A, Kuhlemeier C (2012) Mechanical regulation of auxin-mediated growth. Curr Biol **22:** 1468–1476

Nikovics K, Blein T, Peaucelle A, Ishida T, Morin H, Aida M, Laufs P (2006) The balance between the MIR164A and CUC2 genes controls leaf margin serration in *Arabidopsis*. Plant Cell **18:** 2929–2945

Oikawa T, Kyozuka J (2009) Two-step regulation of *LAX PANICLE1* protein accumulation in axillary meristem formation in rice. Plant Cell **21:** 1095–1108

Quevillon E, Silventoinen V, Pillai S, Harte N, Mulder N, Apweiler R, Lopez R (2005) InterProScan: protein domains identifier. Nucleic Acids Res **33:** W116–W120

Rozen S, Skaletsky HJ (2000) Primer3 on the WWW for general users and for biologist programmers. Methods Mol Biol **132:** 365–386

Ruzin SE (1999) Plant Microtechnique and Microscopy. Oxford University Press, New York

Schmitz G, Theres K (2005) Shoot and inflorescence branching. Curr Opin Plant Biol **8:** 506–511

Sylvester AW, Cande WZ, Freeling M (1990) Division and differentiation during normal and *liguleless-1* maize leaf development. Development **110:** 985–1000

Tavakol E, Okagaki R, Verderio G, Shariati JV, Hussien A, Bilgic H, Scanlon MJ, Todt NR, Close TJ, Druka A, et al (2015) The barley *Uniculme4* gene encodes a BLADE-ON-PETIOLE-like protein that controls tillering and leaf patterning. Plant Physiol **168:** 164–174

Trivett CL, Evert RF (1998) Ontogeny of the vascular bundles and contiguous tissues in the barley leaf blade. Int J Plant Sci **159:** 716–723

Van Ooijen JW (2006) JoinMap 4, software for the calculation of genetic linkage maps in experimental populations. Kyazma, Wageningen, The Netherlands

Wang Q, Hasson A, Rossmann S, Theres K (2016) Divide et impera: boundaries shape the plant body and initiate new meristems. New Phytol **209:** 485–498

Wang Y, Li J (2008) Molecular basis of plant architecture. Annu Rev Plant Biol **59:** 253–279

Wenzel CL, Chandler PM, Cunningham RB, Passioura JB (1997) Characterization of the leaf epidermis of barley (*Hordeum vulgare* L. 'Himalaya'). Ann Bot **79:** 41–46

Wu S, Zhang Y (2007) LOMETS: a local meta-threading-server for protein structure prediction. Nucleic Acids Res **35:** 3375–3382

Yang F, Wang Q, Schmitz G, Müller D, Theres K (2012) The bHLH protein ROX acts in concert with *RAX1* and *LAS* to modulate axillary meristem formation in Arabidopsis. Plant J **71:** 61–70

Žádníková P, Simon R (2014) How boundaries control plant development. Curr Opin Plant Biol **17:** 116–125